Pressure-induced valence changes in mixed-valent systems

1992 J. Phys.: Condens. Matter 4 7067

(http://iopscience.iop.org/0953-8984/4/34/007)

J. Phys.: Condens. Matter 4 (1992) 7067–7094. Printed in the UK

Pressure-induced valence changes in mixed-valent systems

Leena Chandran†, H R Krishna-murthy and T V Ramakrishnan
Department of Physics, Indian Institute of Science, Bangalore 560012, India

Received 7 April 1992

Abstract. Mixed-valent systems based on Ce, Sm, Eu and Yb exhibit a wide range of behaviour with respect to valence changes under the application of pressure. We present a semi-phenomenological model for this behaviour based on competition effects between the usual elastic energy cost and the magnetic energy gain due to valence fluctuations. For the latter we use a mean-field Anderson lattice description and incorporate the effects of pressure by introducing a volume dependence to the Anderson model parameters ϵ_f and Δ. In contrast to existing models such as the Kondo Volume Collapse theory of Allen and Martin, which describes magnetic to non-magnetic transitions without sizable valence change (e.g. γ-Ce→ α-Ce), the Anderson lattice model developed here describes systems with both small and large valence changes: the transition can be continuous (e.g. $EuPd_2Si_2$) or discontinuous ($EuPd_2Si_2$ alloyed with Au).

1. Introduction and experimental overview

The valence (f-electron count) and its dependence on pressure, in mixed-valent rare-earth systems, are extremely sensitive to details of the system. This fact is well illustrated by the difference in the behaviour of the valence of Eu with pressure in three compounds, $EuPd_2Si_2$, $EuNi_2P_2$ and $EuCu_2Si_2$ (Perscheid *et al* 1985), all of which have the same crystal structure ($ThCr_2Si_2$, $I4/mmm$, $Z = 2$). In this paper we present a model capable of providing a unified description of isostructural valence-change transitions, continuous as well as discontinuous, involving both large and small changes in valence, in systems based on Ce, Sm, Eu and Yb. In these systems the rare-earth ion fluctuates between two ionic configurations, f^n and f^{n-1}, only one of which is magnetic. The magnetic energy gained from these fluctuations is a sensitive function of volume, owing to the large difference in the atomic volumes of the two valence configurations. Application of pressure leads to competition effects between the cost in elastic energy and the gain in magnetic energy, giving rise to either continuous or discontinuous valence-change transitions. Since there is no accompanying change in lattice symmetry, the reason for the transitions is simply a bulk-modulus instability. In Sm and Yb based systems, increasing pressure drives the transition from a non-magnetic, high-volume state towards a magnetic (degenerate), low-volume state ($f^6 \rightarrow f^5$ in Sm and $f^{14} \rightarrow f^{13}$ in Yb; the valence changes from 2^+ to 3^+ in both). In the case of Ce and Eu based compounds, the non-magnetic state has a smaller volume and pressure drives the transition from $f^1 \rightarrow f^0$ in Ce (valence 3^+ to 4^+) and $f^7 \rightarrow f^6$ in Eu (valence 2^+ to 3^+).

† Present address: Theoretische Physik, ETH Hönggerberg, Ch-8093 Zürich, Switzerland.

0953-8984/92/347067+28$04.50

We use the Anderson lattice model, treated as a collection of independent Anderson impurities (Anderson 1961), to describe the mixed-valent behaviour in these rare-earth systems. In doing so we neglect inter-site and coherence effects due to the lattice, assuming these are not pressure-dependent. Furthermore, we treat the orbitally degenerate $U = \infty$ version of the Anderson impurity Hamiltonian only within a mean-field approximation of the slave-boson functional-integral technique (Coleman 1984, Read and Newns 1983a,b). Such a description corresponds to taking the $N \rightarrow \infty$ limit of a perturbation expansion in which $1/N$ ($N \equiv$ degeneracy) is used as an expansion parameter (Anderson 1981). The large orbital degeneracy of the magnetic state not only enhances the magnetic energy gained due to valence fluctuations (increased entropy) but also reduces the importance of inter-site contributions ($O(1/N)$) relative to the on-site valence-fluctuation energy (Ramakrishnan 1981), thus providing further justification for neglecting inter-site effects. In order to simulate pressure effects we take the impurity parameters ϵ_f and Δ, the f-level position and the hybridization width respectively, to be volume-dependent.

A similar approach, based on a volume-dependent magnetic energy, has been used earlier by Allen and Martin (1982) and Martin and Allen (1983, 1985) to model the discontinuous γ–α transition in cerium. The transition is discontinuous and is accompanied by a large (15%) change in volume but only a relatively small change in valence (3^+ to 3.3^+ at most). Focusing on the small change in the valence of cerium, they described the transition using a Kondo lattice model with a volume-dependent Kondo coupling constant J. Our model extends their description to include systems that show large or small, discontinuous or continuous changes in valence, e.g. $CeAl_2$ (Vedel *et al* 1986) and $CeCu_2Si_2$ (Spain *et al* 1986), which are among cerium based compounds showing continuous transitions. It is now generally accepted that all cerium systems are nearly integral-valent (valence in the range 3^+–3.2^+) (Wohlleben and Rohler 1984) but their valence changes with pressure can be either continuous or discontinuous (Leger *et al* 1985). Based on spectroscopic studies, Croft *et al* (1981) have suggested that Ce systems be described in terms of a change in the hybridization width Δ (or equivalently the Kondo coupling J) with pressure rather than a shift in f-level position ϵ_f.

In contrast, the valences of Eu, Sm and Yb in their compounds are in the mixed-valent regime. All of them usually show a larger overall change in valence with pressure compared to Ce but the details of their response differ considerably from each other. The chalcogenides of Sm, SmSe and SmTe (Jayaraman *et al* 1974) show continuous valence changes in the mixed-valent regime, while SmS shows the famous 'black to gold', discontinuous, first-order transition at 8 kbar (Chatterjee *et al* 1972). Yb chalcogenides have P–V curves that are rather anomalous compared to other Yb systems, in that they seem to be on the verge of a discontinuous transition. The valence changes with pressure in these materials are rapid (though still continuous) over the range 100–200 kbar (Jayaraman *et al* 1974). The chalcogenides of Eu all show gentle, continuous, valence changes, but two other Eu based systems, EuO and $EuPd_2Si_2$, have very unusual behaviour. EuO is the only Eu based system that shows a first-order valence-change transition (Jayaraman 1972). In $EuPd_2Si_2$ there is an anomalously large variation in the isomer shift (valence) with temperature in the region of 150 K (Croft *et al* 1982a, Holland-Moritz 1985, Sampathkumaran *et al* 1981, Sampathkumaran 1981). Under pressure this large overall change in the isomer shift reduces considerably (Schmiester *et al* 1982), while alloying with Au even drives the transition first-order. The compressibility of this material (Batlogg *et al* 1982) is also

very different from that of Ce (Evdokimova and Genshaft 1965), a fact that can be explained quite naturally within our model. We have found that valence changes in the mixed-valent regime can be understood by allowing for a pressure-dependent shift in the f-level position ϵ_f. Even in the case of YbCuAl, which is a good Kondo system (Hewson *et al* 1985), experimental evidence indicates that the dominant pressure effect is an increase in ϵ_f (Mattens *et al* 1980, Mignot and Wittig 1982).

Another experimental result relevant to our discussion is the fact that the bulk moduli B of mixed-valent compounds in a rare-earth series, e.g. $REAl_2$, REB_6, etc, are much softer than that of their integral-valent counterparts (Jayaraman 1979, King *et al* 1981, Leger *et al* 1985, Penney *et al* 1981). In the integral-valent materials, B as a function of Q/V (where Q is the charge of the rare-earth ion and V the unit-cell volume) is known to follow a linear relationship (Neumann *et al* 1982). The mixed-valent systems fall below this line, indicating that they have a smaller bulk modulus (larger compressibility). This feature, as we shall see below, arises from the fact that in these materials there is a contibution to the effective bulk modulus from valence fluctuations, which is always negative.

Although we discuss the case of hydrostatic pressure, our semi-phenomenological analysis would also apply to the effects of chemical presure, provided local environment effects can be ignored. The effective pressure produced by alloying (McWhan and Remeika 1970) can be positive or negative depending on whether the substituted ion has a size smaller or larger than the host ion. Thus, alloying $EuPd_2Si_2$ with Au, which corresponds to applying negative pressure because the Au ion is larger than that of Pd, gives access to a region of first-order phase transitions in the alloy system $Eu(Pd_{1-x}Au_x)_2Si_2$ (Croft *et al* 1982b, Gupta *et al* 1982, Segre *et al* 1982). That such a first-order phase boundary exists was first proposed by Batlogg *et al* (1982), on the basis of resistivity and Mössbauer experiments. The ability to generate negative pressures makes alloying a very useful tool in the study of phase transitions since it provides access to parts of the phase diagram not available to hydrostatic pressure. Several other interesting results have been obtained in alloy systems. These include the observation and characterization of the critical point in $Ce_{1-x}Th_x$ alloys (Lawrence *et al* 1975), the observation of a second critical point in the same system (Thompson *et al* 1983) and the occurrence of a first-order phase transition in a Yb based system $Yb_xIn_{1-x}Cu$ (Nowik 1986, 1987).

The small cross section of experimental results we have discussed so far have already demonstrated the need for a theoretical description that goes beyond the Kondo Volume Collapse (KVC) model of Allen and Martin. In the following sections we show that, in order to extend their model to encompass all the phenomena we have discussed so far, it is sufficient to replace their Kondo lattice model and volume-dependent coupling J by the Anderson lattice Hamiltonian in which both parameters, ϵ_f and Δ, vary independently with volume. We begin by describing in some detail our treatment of the Anderson model for the description of valence fluctuations in these systems (section 2). In sections 3 and 4, we go on to discuss the predictions of our model, with regard to the nature of phase transitions, assuming various forms for the volume dependences of ϵ_f and Δ. One of these leads to the Kondo Volume Collapse description of Allen and Martin. In section 5 we describe their picture in detail and also our own study of the γ–α transition in cerium. Finally, we discuss the applicability of our model to real systems and comment on the possible consequences of including some of the features left out in our model.

2. Model

We take the Helmholtz free energy for the rare-earth system to be

$$F = \tfrac{1}{2}B_N V_N(\overline{V}-1)^2 + N_i F_i(\epsilon_f, \Delta, T, D). \tag{1}$$

The first term is the elastic energy contribution, for which we have chosen a simple form that yields a linear pressure–volume relationship. B_N is the bulk modulus and V_N the normal volume; $\overline{V} \equiv V/V_N$. The second term is the magnetic energy contribution, where F_i is the magnetic energy of a single Anderson impurity and N_i the number of such impurities. The single-impurity model describes the scattering of conduction electrons from a magnetic impurity (all the f-electron orbitals of the impurity are replaced by a single degenerate orbital) and is characterized by the position and width of the impurity scattering resonance (ϵ_f and Δ) as well as the conduction-electron bandwidth D. Since we assume that ϵ_f and Δ are volume-dependent, the pressure and effective bulk modulus are given by

$$P(T,\overline{V}) \equiv -\frac{\partial F}{\partial V} = B_N(1-\overline{V}) - \frac{N_i}{V_N}\left(\frac{\partial F_i}{\partial \epsilon_f}\frac{\partial \epsilon_f}{\partial \overline{V}} + \frac{\partial F_i}{\partial \Delta}\frac{\partial \Delta}{\partial \overline{V}}\right) \tag{2}$$

$$B(T,\overline{V}) \equiv -\frac{\partial P}{\partial \overline{V}} = B_N + \frac{N_i}{V_N}\frac{\partial^2 F_i}{\partial \overline{V}^2}. \tag{3}$$

From simple thermodynamic considerations, a first-order phase transition from volume $\overline{V}_1$ to $\overline{V}_2$, signalled by a bulk-modulus instability, occurs at a transition pressure $P_t(T)$, which pre-empts this instability. The latter is determined from

$$P_t(T) = P(T,\overline{V}_1) = P(T,\overline{V}_2) \tag{4}$$

and

$$G(T,P_t) \equiv F(T,\overline{V}_1) + P_t(T)\overline{V}_1 = F(T,\overline{V}_2) + P_t(T)\overline{V}_2. \tag{5}$$

These are just the conditions for the pressure and Gibbs free energies of the two phases to be equal. The phase boundary, given by $P_t(T)$, can be terminated by (upper and/or lower) critical temperatures at which the effective bulk modulus is zero and $\overline{V}_1$ coincides with $\overline{V}_2$. Thus the conditions

$$B(T_c,\overline{V}_c) = 0 \tag{6}$$

and

$$\partial B(T_c,\overline{V}_c)/\partial \overline{V} = 0 \tag{7}$$

determine the critical points T_c and $\overline{V}_c$.

For an explicit form of the impurity free energy, $F_i(\epsilon_f, \Delta, T, D)$, we use results from a new formulation of large-N slave-boson mean-field theory (Chandran 1987, Chandran and Krishna-murthy 1987) in which, unlike the conventional formulation, thermodynamic properties can be calculated over a large range of temperatures of interest, across and beyond the Kondo temperature. For completeness, we summarize

below the salient features of the conventional large-N slave-boson treatment for the Anderson impurity model in the $U = \infty$ limit as well as our modification of it. The Hamiltonian is written as (Coleman 1984)

$$H = \sum_{k,m} \epsilon_k c_{km}^+ c_{km} + \sum_m \epsilon_{fm} f_m^+ f_m + \frac{V}{\sqrt{N}} \sum_{k,m} (c_{km}^+ b^+ f_m + f_m^+ b c_{km}) \tag{8}$$

where b^+ and b are auxiliary (slave) boson operators introduced in the slave-boson technique, to represent the impurity orbital in its empty state. The c and f operators, both of which carry a degeneracy index, are fermions representing the conduction electrons and the single electron occupying the magnetic impurity orbital respectively. The $U = \infty$ constraint condition (U being the on-site correlation energy) restricts the charge Q on the impurity orbital to be 1 and is expressed as

$$Q \equiv \sum_m f_m^+ f_m + b^+ b = 1. \tag{9}$$

Within the functional-integral treatment (Read and Newns 1983a,b), this constraint condition is incorporated as an integral over a Lagrange multiplier field λ in the partition function (Z_+):

$$Z_+ = \int_{-\pi/\beta}^{\pi/\beta} \frac{\beta}{2\pi} \mathrm{d}\lambda \, \mathrm{Tr}\{\exp[-\beta H - \mathrm{i}\beta\lambda(Q-1)]\}. \tag{10}$$

The trace is then rewritten as integrals over (imaginary-time) auxiliary boson fields as well as Grassman fields corresponding to the fermions. A mean-field (leading order in a $1/N$ expansion) approximation consists of making, first, the static approximation for the bose fields, i.e. $b^*(\tau) = b(\tau) = b_0$. The action functional and the partition function (in the static limit and after integrating out the fermion fields) are then

$$Z_+ = Z_c \int \exp[-S(b_0^2, \lambda, T)] \tag{11}$$

and

$$S(b_0^2, \lambda, T) = \beta N \left[(b_0^2 - q_0)\lambda + \frac{\tilde{\epsilon}_f}{2} + T \ln \left(\frac{\tilde{\Gamma}(z)\tilde{\Gamma}(z^*)}{2\pi} \right) + \frac{\tilde{\Delta}}{\pi} \ln \left(\frac{2\pi T}{D} \right) \right]. \tag{12}$$

Here,

$$\tilde{\Gamma}(z) = \tilde{\Gamma}\left(\tfrac{1}{2} + \beta\xi/2\pi\mathrm{i}\right) \qquad \text{and} \qquad \xi = \tilde{\epsilon}_f + \mathrm{i}\tilde{\Delta} \tag{13}$$

with

$$\tilde{\epsilon}_f = \epsilon_f + \lambda \qquad \tilde{\Delta} \equiv \pi\rho V^2 b_0^2 \equiv \Delta b_0^2 \qquad q_0 = 1/N. \tag{14}$$

Z_c, the conduction-electron contribution, is the partition function of a non-interacting electron gas. Within conventional mean-field theory, the next step is to write the free

energy as the classical saddle-point value of the action. Thus $\beta F_i = S(b_c^2, \tilde{\lambda}, T)$, where b_c^2 and $\tilde{\lambda}$ are determined from the stationary-point conditions

$$\partial S/\partial \lambda = 0 \qquad \text{and} \qquad \partial S/\partial b_0 = 0. \tag{15}$$

These translate into

$$\tilde{\Psi}(Z) + \ln(2\pi T/D) + \lambda\pi/\Delta + i\pi(\tfrac{1}{2} - q_0 + b_0^2) = 0 \tag{16}$$

$\tilde{\Psi}(Z)$ being the digamma function. The above equation yields a temperature-dependent solution, $\xi(T) = \tilde{\epsilon}_f(T) + i\tilde{\Delta}(T)$, which describes a Lorentzian scattering resonance of width $\tilde{\Delta}$ at position $\tilde{\epsilon}_f$. At a temperature T_c defined by the condition $\tilde{\Delta}(T_c) = 0$, conventional mean-field theory breaks down. F_i can no longer be approximated as the saddle-point value of the action and calculation of physical quantities cannot be extended beyond this temperature. Since this temperature is only of the order of the Kondo temperature, defined here as

$$T_K \equiv (\tilde{\epsilon}_f^2 + \tilde{\Delta}^2)^{1/2} \tag{17}$$

most of the temperature range of interest in the problem (up to 100 times T_K), from the point of view of valence-change transitions, is excluded from study by this method.

We have modified the conventional mean-field theory slightly, in order to obtain a working prescription for calculating thermodynamic properties over the range of temperatures of interest. In our prescription, we retain the static approximation but deviate from the saddle-point approximation partially to calculate the partition function Z as a weighted integral over all allowed static values of the bose field b_0^2 (Chandran 1987, Chandran and Krishna-murthy 1987):

$$Z = Z_c \int_{b_0^2} \exp[-S(b_0^2, \tilde{\lambda}, T)]. \tag{18}$$

Of the two saddle-point conditions in (15), we have relaxed the latter ($\partial S/\partial b_0 = 0$) so that b_0^2 is no longer determined by its classical value b_c^2. For every static value of b_0^2, $\tilde{\lambda}(b_0^2, T)$ is, as before, determined from the first extremum condition in (15), i.e. $\partial S/\partial \lambda = 0$. This ensures that the constraint is imposed on the average, i.e. (using $n_f \equiv \partial F_i/\partial \epsilon_f$ and $\beta F_i = S$),

$$n_f = \tfrac{1}{2} + (1/\pi)\mathrm{Im}\,\tilde{\Psi}(Z) = q_0 - b_0^2. \tag{19}$$

The above condition also fixes the upper limit on the range of integration over b_0^2 to be q_0, which corresponds to the minimum value of the valence ($n_f = 0$). Since calculation of the partition function itself involves an integral over the amplitude of the bose field, physical quantities are now also to be obtained as weighted averages over Boltzmann factors corresponding to different static values of b_0^2, analogous to the calculation of expectation values. For example, the valence and its derivative with respect to ϵ_f are given by

$$n_f \equiv \frac{\partial F_i}{\partial \epsilon_f} = \frac{k_B T}{Z} \int_{b_0^2} e^{-\beta F} \frac{\partial(\beta F)}{\partial \epsilon_f} = k_B T \left\langle \frac{\partial S}{\partial \epsilon_f} \right\rangle \tag{20}$$

and

$$\partial^2 F_i/\partial\epsilon_f^2 = k_B T\left[\langle \partial S/\partial\epsilon_f\rangle^2 + \langle \partial^2 S/\partial\epsilon_f^2\rangle - \langle(\partial S/\partial\epsilon_f)^2\rangle\right]. \quad (21)$$

At low temperatures, the maximum contribution to Z as well as physical quantities comes from values of b_0^2 in the neighbourhood of the classical value b_c^2. At $T = 0$ itself, only b_c^2 contributes and the free energy is again $\beta F_i = S(b_c^2, \tilde{\lambda}, T)$ as in the conventional mean-field theory. Thus, our prescription differs from the latter only at non-zero temperatures.

Returning now to the discussion of valence-change transitions, we point out a few noteworthy facts. (i) The singlet and the multiplet f configurations of the impurity are replaced, in the model, by a single degenerate orbital in which the occupation number is restricted to be either 0 or 1 by the constraint condition. Thus valence 1 in our model corresponds to the f^6 configuration and valence 2^+ in Sm systems, to the f^1 configuration and valence 3^+ in Ce systems, and so on. (ii) The temperature dependence of the Helmholtz free energy F (cf equation (1)), in our model, comes entirely from the impurity contribution F_i. (iii) Since the elastic contribution to F is assumed to be such that it gives a linear pressure–volume relationship, any non-linearity in the P–V behaviour would again have to come from F_i. Various other forms for the elastic energy contribution have been suggested in the literature. We have made preliminary studies with one other form (Rose *et al* 1984), but find that this does not change, qualitatively, any of the conclusions we have presented here based on the simple form in (1).

In the next two sections we describe results obtained from assuming a linear volume dependence, separately, for ϵ_f and Δ. We first consider the case when ϵ_f varies linearly with volume as

$$\epsilon_f(\overline{V}) = \epsilon_f(0) + \delta D(1 - \overline{V}) \quad (22)$$

where $\epsilon_{f0} \equiv \epsilon_f(0) = -0.5D$ and Δ is held fixed at $\Delta_0 = 0.08D$. From analytical estimates at zero temperature, we show that the model then describes valence changes centred around $n_f = 2/3$, i.e. in the mixed-valent regime. Next we study the case when Δ varies linearly as

$$\Delta(\overline{V}) = \Delta_0 - \alpha D(1 - \overline{V}) \quad (23)$$

where $\Delta_0 = 0.08D$ and ϵ_f is held fixed at $\epsilon_{f0} = -0.5D$. Again from a $T = 0$ analysis, it is easy to show that now valence changes are confined to the Kondo regime and lead quite naturally to a Kondo Volume Collapse type of interpretation. We have also studied two other cases: (i) when both ϵ_f and Δ vary simultaneously with volume, linearly; and (ii) when ϵ_f varies non-linearly with volume for fixed Δ.

It is worth emphasizing that, even when we assume a linear volume dependence for ϵ_f or Δ, the free energy and its volume derivatives, the pressure and bulk modulus, have a highly non-linear dependence on volume through their non-linear dependence on these parameters. This non-linearity is in fact responsible for driving a first-order valence-change transition.

3. Mixed-valent regime

When only ϵ_f varies with volume according to (22), Δ being fixed at $\Delta_0 = 0.08D$, the normalized (dimensionless) pressure and bulk modulus defined as

$$\overline{P} \equiv PV_N/N_i D \quad (24)$$

$$\overline{B} \equiv BV_N/N_i D \tag{25}$$

are given by (cf equations (2) and (3))

$$\overline{P} = \overline{B}_N(1-\overline{V}) + (\partial F_i/\partial \epsilon_f)\delta \tag{26}$$

$$\overline{B} = \overline{B}_N + (\partial^2 F_i/\partial \epsilon_f^2)\delta^2 D. \tag{27}$$

Since ϵ_f depends linearly on volume, one can use (22) to replace $(1-\overline{V})$ by $(\epsilon_f - \epsilon_{f0})/\delta D$ in (26) to obtain pressure as a function of ϵ_f, which is essentially the equation of state. We first consider the situation at zero temperature, when the ϵ_f derivatives of the free energy in equations (26) and (27) can be evaluated analytically. The impurity free-energy functional at zero temperature, obtained from the $T = 0$ limit of (12), is

$$F_i = N\left[(b_0^2 - q_0)\tilde{\lambda} + \frac{\tilde{\Delta}}{2\pi}\ln\left(\frac{\tilde{\Delta}^2 + \tilde{\epsilon}_f^2}{D}\right) - \frac{\tilde{\Delta}}{\pi} + \frac{\tilde{\epsilon}_f}{\pi}\tan^{-1}\left(\frac{\tilde{\Delta}}{\tilde{\epsilon}_f}\right)\right]. \tag{28}$$

In the $N \to \infty$ limit, the values of b_0^2 (at $T = 0$ this is the classical value b_c^2, and henceforth we will denote it only as b_0^2, since the distinction between b_c^2 at zero temperature and b_0^2, to be integrated over, at finite temperatures will always be clear from the context) and $\tilde{\lambda}$ that minimize this functional are determined by the zero-temperature limit of the saddle-point conditions

$$\tilde{\lambda} = \Delta_0 \ln(D/\tilde{\epsilon}_f) + O(1/N^2) \tag{29}$$

$$|b_0^2| = \frac{1}{N}\frac{\tilde{\epsilon}_f}{\tilde{\epsilon}_f + \Delta_0}. \tag{30}$$

The actual free energy F_i is simply evaluated at these values of b_0^2 and $\tilde{\epsilon}$. Then the valence n_f is given by

$$n_f \equiv \partial F_i/\partial \epsilon_f = \Delta_0/(\tilde{\epsilon}_f + \Delta_0) \tag{31}$$

while

$$\partial^2 F_i/\partial \epsilon_f^2 = -\Delta_0 \tilde{\epsilon}_f/(\tilde{\epsilon}_f + \Delta_0)^3. \tag{32}$$

(To derive these, the implicit dependence of $\tilde{\lambda}$ on ϵ_f through the saddle-point condition (29) has to be included.) Furthermore,

$$\frac{\partial^3 F_i}{\partial \epsilon_f^3} = \frac{\Delta_0 \tilde{\epsilon}_f}{(\tilde{\epsilon}_f + \Delta_0)^5}(2\tilde{\epsilon}_f - \Delta_0). \tag{33}$$

Now consider the impurity contribution to the bulk modulus in (27). From (32) it is clear that this is always negative and has its lowest value, i.e. is most negative, when

$$\partial^3 F_i/\partial \epsilon_f^3 = 0 \tag{34}$$

i.e. when

$$\tilde{\epsilon}_f = \Delta_0/2 \qquad \text{or} \qquad \epsilon_f = \epsilon_{fc} \equiv \Delta_0\left[\tfrac{1}{2} - \ln(2D/\Delta_0)\right]. \tag{35}$$

At this minimum

$$n_f = \tfrac{2}{3} \qquad \text{and} \qquad \partial^2 F_i/\partial\epsilon_f^2 = -4/(27\Delta_0). \tag{36}$$

This is clearly the mixed-valent regime where n_f is changing most rapidly with ϵ_f. On either side of this $|\partial^2 F_i/\partial\epsilon_f^2|$ decreases and tends to zero. For $-\epsilon_f \gg \Delta_0$, i.e. deep in the Kondo regime,

$$\tilde{\epsilon}_f \simeq D\exp(\epsilon_f/\Delta_0) \equiv T_0 \tag{37}$$

and

$$\partial^2 F_i/\partial\epsilon_f^2 \simeq -T_0/\Delta_0^2. \tag{38}$$

For $\epsilon_f \gg \Delta_0$, in the strongly mixed-valent regime,

$$\tilde{\epsilon}_f = \epsilon_f + \Delta_0 \ln(D/\epsilon_f) \tag{39}$$

and

$$\partial^2 F_i/\partial\epsilon_f^2 \simeq -\Delta_0/\epsilon_f^2. \tag{40}$$

Thus as the volume varies, and with it ϵ_f, the bulk modulus $\overline{B}$ is always less than $\overline{B}_N$, and attains its minimum value of

$$\overline{B}_{min} = \overline{B}_N - [4/(27\Delta_0)]\delta^2 D \tag{41}$$

when $\epsilon_f = \epsilon_{fc}$. Clearly, unless δ is bigger than a critical value $\delta_c(0)$ given by

$$\delta_c^2(0) = (27/4)\overline{B}_N/(D/\Delta_0) \tag{42}$$

$\overline{B}$ is always positive and *there is never a bulk-modulus instability*. But if $\delta > \delta_c(0)$, there is a range of ϵ_f around ϵ_{fc} (and correspondingly a range of $\overline{V}$) where $\overline{B}$ is negative. Consequently this bulk-modulus instability will be pre-empted by a first-order phase transition with discontinuous volume and valence changes, at a transition pressure determined by the conditions (4) and (5). We note that at the critical point

$$n_{fc}(0) = \tfrac{2}{3} \qquad \text{and} \qquad \overline{P}_c(0) = \overline{B}_N(\epsilon_{fc} - \epsilon_{f0})/\delta_c(0) + \tfrac{2}{3}\delta_c(0). \tag{43}$$

We therefore have an important and interesting result, namely that our model free energy contains the ingredients for obtaining continuous ($\delta < \delta_c(0)$) and discontinuous ($\delta > \delta_c(0)$) valence transitions in the mixed-valent regime centred around $n_f \simeq 2/3$. We believe that this is just the feature needed to understand the behaviour of Eu, Sm and Yb based mixed-valent systems.

A completely analogous discussion to the one given above can be carried out at non-zero temperatures. Now $n_f(V \equiv \partial F_i/\partial\epsilon_f)$ and $\partial^2 F_i/\partial\epsilon_f^2$ are given by (20) and (21) and the integrals have to be done numerically. At any temperature T,

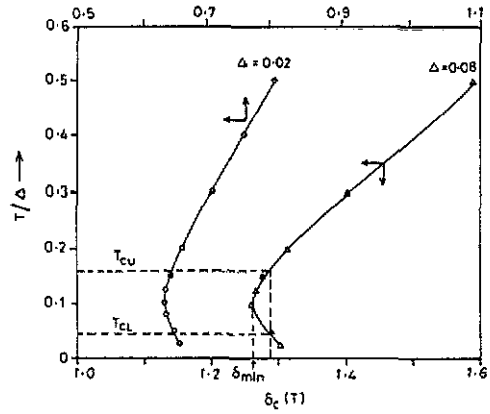

Figure 1. Plot of $\delta_c(T)$, the critical value of the slope of the volume variation of ϵ_f, with temperature for two fixed values of Δ' ($\equiv \Delta_0/D$). At a fixed temperature T a first-order transition occurs only for $\delta > \delta_c(T)$. For each Δ' there is a minimum value of $\delta_c(T)$ ($\equiv (\delta_c)_{min}$) such that for δ between $(\delta_c)_{min}$ and $\delta_c(0)$ there is a first-order phase boundary terminated by two critical points.

$\partial^2 F_i/\partial\epsilon_f^2$ is again negative and has its minimum value at a critical $\epsilon_{fc}(T)$, which must be determined numerically from the condition $\partial^3 F_i/\partial\epsilon_f^3 = 0$. Then the critical $\delta_c(T)$ is determined by

$$\delta_c^2(T) = -\left(\frac{B_N}{D}\right) \Big/ \left(\frac{\partial^2 F_i}{\partial \epsilon_f^2}\right)_{min} . \tag{44}$$

Once again, if $\delta < \delta_c(T)$ there is no bulk-modulus instability, but if $\delta > \delta_c(T)$ there is one, giving rise to a discontinuous transition. Our numerical results for $\delta_c(T)$ are shown in figure 1 for two different (but fixed) values of Δ_0. For each Δ_0 there is a minimum value of $\delta_c(T)$, which we will denote by $(\delta_c)_{min}$, such that for $\delta < (\delta_c)_{min}$ only continuous transitions can occur for the entire range of temperatures. For any fixed value of δ between $(\delta_c)_{min}$ and $\delta_c(0)$ one clearly has upper and lower critical temperatures, T_{cu} and T_{cl}, such that there is a bulk-modulus instability only for $T_{cu} > T > T_{cl}$. Figures 2 and 3 show $\overline{P}$ versus $\overline{V}$ and n_f versus $\overline{V}$ curves respectively for one such fixed value of δ (Δ_0 fixed at $0.08D$) and three values of temperature, two of them close to the upper and lower critical temperatures corresponding to this δ, with the third in between. Typical curves for the bulk modulus as a function of pressure at a fixed temperature and different values of the parameter δ are plotted in figure 4. Curve B is the critical curve at $\delta = \delta_c(T)$. For values of $\delta > \delta_c(T)$ as in curve C, the instability appears, accompanied by a discontinuous change in volume and valence, as discussed earlier. The compressibility $\overline{K} \equiv 1/\overline{B}$ corresponding to curve A in this figure is plotted in figure 5 over a wide range of pressure. The behaviour strongly resembles experimental results in $EuPd_2Si_2$ (Batlogg *et al* 1982). Figure 6 shows a plot of $(1 - n_f)$ versus pressure for a fixed $\delta < (\delta_c)_{min}$ (corresponding to continuous transitions) at several temperatures. It is clear that parts of these curves may be used to model the n_f versus pressure data in mixed-valent systems. For example, the low-pressure part of the curve at $T/T_0 = 0.5$ could be fitted to $YbAl_2$ (Rohler *et al* 1982) or Yb metal (Wortmann *et al* 1982), while parts of the curves for $T/T_0 = 2$ or 4 could be fitted either to SmS in the gold phase or to $EuPd_2Si_2$ (Rohler *et al* 1982). The same data are plotted as a function of volume $(1 - \overline{V})$ in figure 7. The change in behaviour of n_f with $(1 - \overline{V})$ for different parametric values of T/T_0 is similar to the behaviour of the isomer shift with temperature for different pressures in $EuPd_2Si_2$ (Schmiester *et al* 1982).

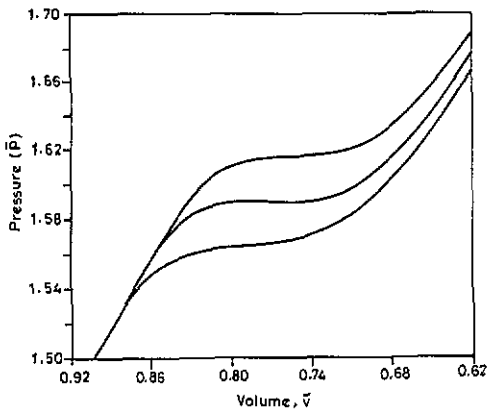

Figure 2. Typical $\overline{P}$ versus $\overline{V}$ curves for a fixed δ (between $(\delta_c)_{min}$ and $\delta_c(0)$) and three values of temperature, two of which are close to the upper and lower critical points appropriate for this δ.

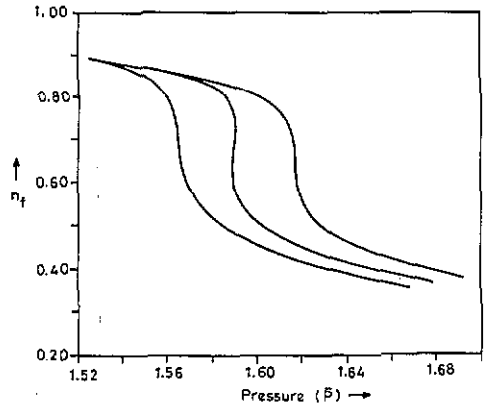

Figure 3. Valence versus pressure for the same fixed δ and the same values of temperature as in figure 2.

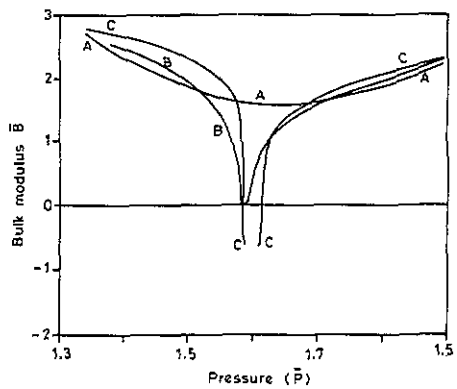

Figure 4. Typical curves for the bulk modulus as a function of pressure at a fixed temperature $(T/\Delta_0 = 0.1)$ for various δ. For $\delta > (\delta_c)_{min}$ (curve C) there is a bulk-modulus instability, $\overline{B}$ becoming negative over a range of pressures that is the first-order phase boundary. Curve B is the critical curve.

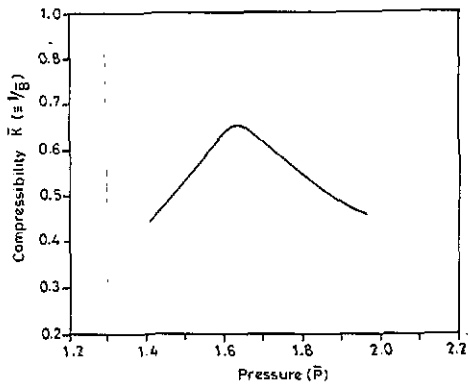

Figure 5. The compressibility $\overline{K} \equiv 1/\overline{B}$ corresponding to curve A in figure 4 is plotted over a wider range of pressure. The behaviour seen here resembles the experimental results in $EuPd_2Si_2$ (Batlogg *et al* 1982).

It is reasonable to expect that the largest continuous variation in valence with temperature would occur for values of δ close to $(\delta_c)_{min}$. That this is indeed true can be seen from figure 8 where n_f versus temperature is plotted for two values of δ less than $(\delta_c)_{min}$, with $\delta_1 < \delta_2 < (\delta_c)_{min}$. The variation in n_f with T is larger and more rapid for δ_2 than for δ_1. This is again similar to the behaviour of the isomer shift with temperature in $EuPd_2Si_2$ (Schmiester *et al* 1982) for different external pressures. Here δ plays the role of pressure. In our model δ is a phenomenological parameter, to be fixed for every system by comparison with experiment. We have also set it to be independent of pressure, but in general it is more likely that δ itself would

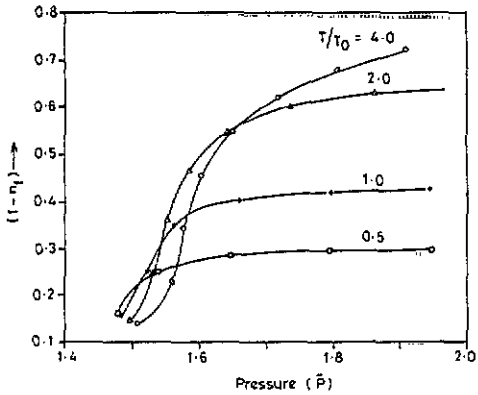

Figure 6. Plot of $(1 - n_f)$ versus pressure for a fixed $\delta < (\delta_c)_{min}$ (only continuous transitions) and several temperatures. It is clear that parts of these curves may be used to model the n_f versus pressure data in mixed-valent systems (see text).

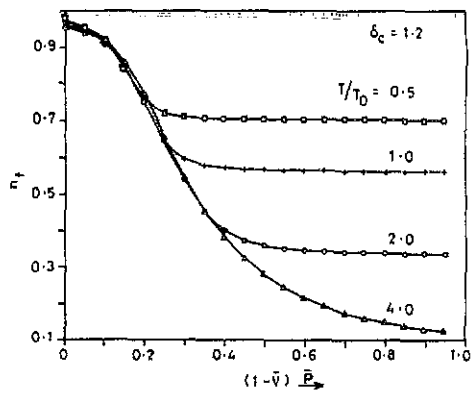

Figure 7. The same data for the valence in figure 6 is plotted here as a function of volume $(1 - \overline{V})$. Notice that the behaviour of n_f with $(1 - \overline{V})$ for different parameter values of T/T_0 is similar to the behaviour of the isomer shift with temperature for different pressures in $EuPd_2Si_2$ (Schmiester *et al* 1982).

be pressure-dependent. Since the lattice stiffens with increasing pressure, its response to a further increase in pressure reduces. Then it would be reasonable to expect that δ, the rate of change of ϵ_f with volume/pressure, would decrease as the pressure increases. Equivalently, this effect amounts to a non-linear volume dependence for the hybridization width ϵ_f. Since we have separately studied a non-linear volume variation of ϵ_f for which we describe our results at the end of the next section, here we keep δ independent of pressure. In spite of this, as emphasized earlier, the free energy depends non-linearly on volume through its non-linear dependence on these parameters.

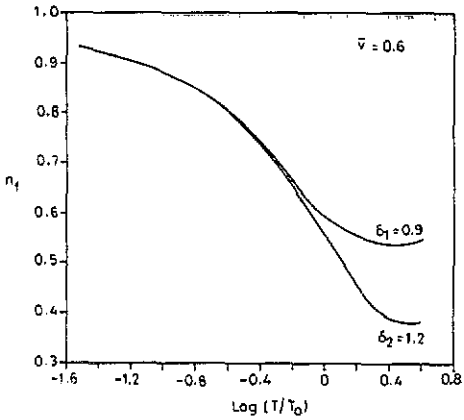

Figure 8. Valence versus temperature for two values of δ close to $(\delta_c)_{min}$ such that $\delta_1 < \delta_2 < (\delta_c)_{min}$. The overall variation in n_f with T is larger for δ_2 than for δ_1, illustrating the fact that the largest continuous variation of valence occurs for δ closest to $(\delta_c)_{min}$.

4. Kondo regime

So far we have discussed the properties of our model free energy when Δ is held fixed and ϵ_f varies linearly with volume. We now consider the circumstance when ϵ_f is held fixed at $\epsilon_f(0) = \epsilon_{f0} = -0.5D$ while Δ varies linearly with volume around $\Delta_0 = 0.08D$ as in (23). Then one has results analogous to the earlier results with $\Delta \to (-\epsilon_f)$ and $\delta \to \alpha$. In particular (compare equations (26) and (27)), the pressure and the bulk modulus are now

$$\overline{P} = \overline{B}_N(\Delta_0 - \Delta)/\alpha D - (\partial F_i/\partial\Delta)\alpha \tag{45}$$

$$\overline{B} = \overline{B}_N + (\partial^2 F_i/\partial\Delta^2)\alpha^2 D. \tag{46}$$

At finite temperatures, the derivatives of F_i with respect to Δ can again be expressed as averages over b_0^2 (compare equations (20) and (21)):

$$\partial F_i/\partial\Delta = k_B T\langle\partial S/\partial\Delta\rangle \tag{47}$$

$$\partial^2 F_i/\partial\Delta^2 = k_B T\left[\langle(\partial S/\partial\Delta)^2\rangle + \langle\partial^2 S/\partial\Delta^2\rangle - \langle(\partial S/\partial\Delta)^2\rangle\right] \tag{48}$$

while at zero temperature analytical estimates can be made, in analogy with equations (31) and (32):

$$\frac{\partial F}{\partial\Delta} = -\frac{\tilde{\epsilon}_{f0} - \epsilon_{f0}}{\Delta_0}\frac{\tilde{\epsilon}_{f0}}{\tilde{\epsilon}_{f0} + \Delta_0} \tag{49}$$

$$\frac{\partial^2 F}{\partial\Delta^2} = \frac{(\tilde{\epsilon}_{f0} - \epsilon_{f0})}{\Delta_0}\frac{\tilde{\epsilon}_{f0}(\epsilon_{f0} + \tilde{\epsilon}_{f0} + 2\Delta_0)}{(\tilde{\epsilon}_{f0} + \Delta_0)^2}. \tag{50}$$

In contrast to $\partial^2 F_i/\partial\epsilon_f^2$ at $T = 0$ (equation (32)), which is always negative, $\partial^2 F_i/\partial\Delta^2$ is negative only deep in the Kondo regime when $-\epsilon_{f0} \gg \Delta_0$. In that regime

$$\tilde{\epsilon}_{f0} \simeq T_0 \equiv D\exp(\epsilon_{f0}/\Delta_0) = D\exp(-1/J) \tag{51}$$

where $J = -\Delta_0/\epsilon_{f0}$ is the dimensionless Kondo coupling constant and T_0 the Kondo temperature. Then

$$\partial^2 F/\partial\Delta^2 \simeq -T_0(1 - 2J)/\epsilon_{f0}^2 J^4 \tag{52}$$

which is indeed negative when $J < 1/2$. On the other hand, in the limit where $\epsilon_{f0} \gg \Delta_0$ one has

$$\tilde{\epsilon}_{f0} \simeq \epsilon_{f0} + \Delta_0 \ln(D/\epsilon_{f0}) \tag{53}$$

whence

$$\partial^2 F/\partial\Delta^2 \simeq (2/\epsilon_{f0})\ln(D/\epsilon_{f0}). \tag{54}$$

Thus when Δ alone varies linearly with volume, our model free energy can develop a bulk-modulus instability only deep in the Kondo regime, where one can equally well talk about a linear variation of J in the form

$$J(V) = J_0 + \alpha'(1 - \overline{V}) \tag{55}$$

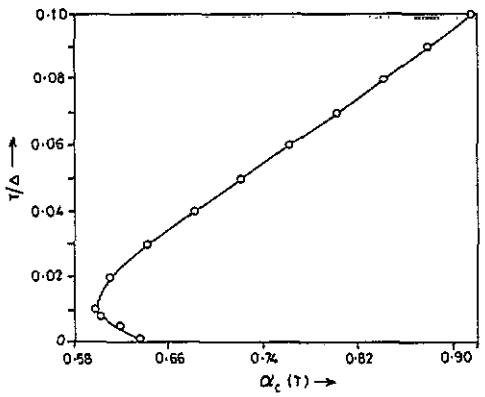

Figure 9. Plot of $\alpha_c(T)$, the critical value of the slope for the volume variation of Δ, as a function of temperature. For $\alpha < \alpha_c(T)$ only continuous transitions occur, but for $\alpha > \alpha_c(T)$ there is a first-order phase boundary.

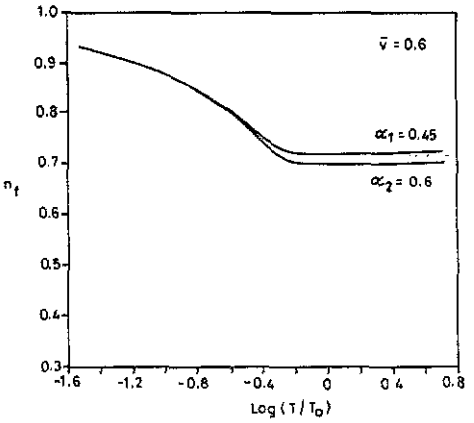

Figure 10. Valence versus temperature for the same fixed volume as in figure 8 but with Δ as the volume-dependent parameter in place of ϵ_f. Notice that in this case the change in n_f is much smaller while the values of n_f are restricted to lie in the integral-valent regime.

where $J_0 = J(0) = -\Delta_0/\epsilon_{f0}$ and $\alpha' = \alpha D/\epsilon_{f0}$. This is exactly the Allen and Martin picture of the γ–α transition in cerium, which we will discuss in detail in the following section. In terms of J

$$\partial F/\partial J = -\epsilon_{f0}\,\partial F/\partial \Delta \simeq -T_0/J^2 \tag{56}$$

$$\partial^2 F/\partial J^2 = \epsilon_{f0}^2\,\partial^2 F/\partial \Delta^2 \simeq -T_0(1-2J)/J^4. \tag{57}$$

As is easily verified, $\partial^2 F/\partial J^2$ has a minimum when $J = J_c = 0.2113$ at which it has a value equal to $-2.55D$. Clearly if $\alpha' > \alpha_c'(0)$ where

$$\alpha_c'^2(0) = \frac{\overline{B}_N D}{(\partial^2 F_i/\partial J^2)_{\min}} = \frac{\overline{B}_N}{2.55} \tag{58}$$

then there is a bulk-modulus instability and an attendant first-order phase transition with a discontinuous volume change: the Kondo Volume Collapse (KVC) transition of Allen and Martin.

As before at finite temperatures, we can use numerical results for $(\partial F/\partial \Delta)$ and $(\partial^2 F/\partial \Delta^2)$, as computed from (47) and (48), to calculate a critical $\alpha_c'(T)$ given by

$$\alpha_c'(T) = \frac{\alpha_c T}{(-\epsilon_{f0}/\Delta)^2} = -\frac{D\overline{B}_N}{\epsilon_f^2(\partial^2 F/\partial \Delta^2)} = -\frac{D\overline{B}_N}{(\partial^2 F/\partial J^2)_{\min}}. \tag{59}$$

Thus at any temperature T, the KVC transition is possible only if $\alpha' > \alpha_c'(T)$. Figure 9 shows the numerical results we have obtained for $\alpha_c(T)$. Note the qualitative similarity between the $\alpha_c(T)$ and the $\delta_c(T)$ curves in figure 1. For any fixed ϵ_{f0} there exists an $(\alpha_c)_{\min}$ such that for $\alpha < (\alpha_c)_{\min}$ only continuous transitions occur. For $(\alpha_c)_{\min} < \alpha < \alpha_c(0)$, there are upper and lower critical temperatures such that for $T_{cu} > T > T_{cl}$ one has the first-order KVC transition as the volume/pressure changes.

Since the above considerations are applicable only in the Kondo regime, the corresponding valence changes are very small. This is illustrated in figure 10 where the valence is plotted as a function of temperature for the same fixed volume as in figure 8 and two values of α less than but close to $(\alpha_c)_{min}$. In contrast to figure 8, where the overall valence changes are large and span all of the mixed-valent regime, the changes here are much smaller and cover only the integral-valent regime. Note also the trend that smaller values of α, i.e. further away from $(\alpha_c)_{min}$, correspond to smaller overall changes. Thus, the only difference between the two separate volume variations is the fact that one of them describes small valence changes in the Kondo (integral-valent) regime while the other covers large valence changes in the mixed-valent regime. Both are capable of describing continuous as well as discontinuous transitions.

Next we consider the situation when ϵ_f and Δ are both varying linearly with volume according to (22) and (23). This simultaneous volume dependence will obviously be present in many mixed-valent systems and we expect that the behaviour in such cases will interpolate between the two extreme limits we have just discussed. In particular, for any fixed temperature, instead of a critical $\alpha_c(T)$ or $\delta_c(T)$, there will now be a critical line in the δ–α plane on one side of which there is a bulk-modulus instability. This critical line is shown in figure 11 at zero temperature. The corresponding critical values of the valence, volume and pressure vary smoothly along this curve, the valence varying from 2/3 for $\delta \neq 0$, $\alpha = 0$ to a value close to 1 at $\delta = 0$, $\alpha \neq 0$. The shaded region in the figure represents the range of values of δ and α for which discontinuous transitions can occur at $T = 0$.

Finally it is interesting to examine the results from a non-linear volume dependence of the Anderson model parameters. In particular, consider a volume dependence of ϵ_f of the form

$$\epsilon_f(V) = \epsilon_f(0)/\overline{V}^n \tag{60}$$

with Δ held fixed at $\Delta_0 = 0.08D$ and both $\epsilon_f(V)$ and $\epsilon_f(0)$ taking negative values. While experiments suggest values of n between -4 and -10 (Schilling 1979), we have studied a smaller value of $n = -2$ in order to be able to observe trends with increasing non-linearity. Since $\epsilon_f(0)$ is negative, $n = -2$ implies that $\epsilon_f(V)$ increases with pressure, becoming less negative (closer to the Fermi level). Now there is an $\epsilon_{fc}(T)$ (analogous to $\delta_c(T)$ and $\alpha_c(T)$), which is the critical value of $\epsilon_f(0)$ (for fixed n) at temperature T, beyond which a first-order transition occurs. The results for $\epsilon_{fc}(T)$ are shown in figure 12. It is interesting to compare the behaviour of valence as a function of pressure or volume for the linear and non-linear volume variation of ϵ_f. For $\overline{V}$ close to 1, the latter can be approximated as

$$\epsilon_f(\overline{V}) = \epsilon_f(0)[1 - n(1 - \overline{V})] \tag{61}$$

which corresponds to a linear variation of the form (22) with $\delta = -n(\epsilon_f/D)$. We have used this value of δ in the linear variation (for all $\overline{V}$) for making the comparison. Figures 13 and 14 show plots of valence versus pressure at four different temperatures in the two cases. The initial response to pressure ($\overline{P}$ in the range 1 to 1.6) is more sensitive in the non-linear case at all temperatures, the valence changing rapidly with pressure. At low temperatures the change in n_f is larger and saturates at a lower pressure in the non-linear case, but this trend is reversed at higher temperatures. The

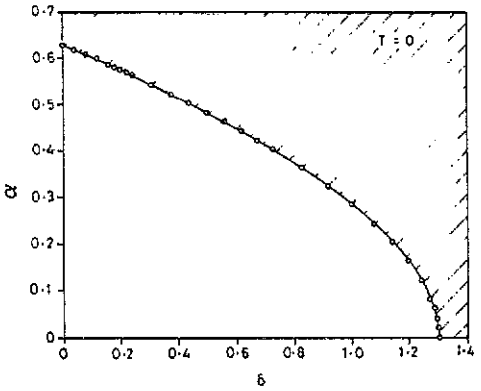

Figure 11. In the case of a combined variation of ϵ_f and Δ with volume, at any particular temperature there now exists a critical line in the δ–α plane. The shaded region represents the range of values of δ and α over which a discontinuous transition can occur at $T = 0$.

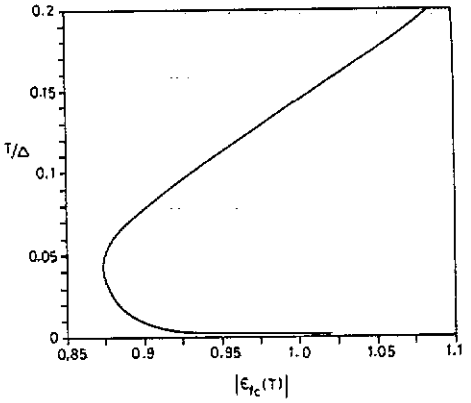

Figure 12. Plot of $\epsilon_{fc}(T)$, the critical value of $\epsilon_f(0)$ at temperature T, for a non-linear volume variation of ϵ_f, beyond which a first-order transition occurs.

reversal of trends is better illustrated in figure 15 where the triangles correspond to the non-linear and circles to the linear volume dependence of ϵ_f. While at $T = 0.5T_0$ (open symbols) the non-linear behaviour shows a faster variation accompanied by large changes in n_f, at $T = 4T_0$ (full symbols) it is the linear dependence that gives a larger variation. The overall change in valence with temperature is larger in the case of the linear variation of ϵ_f, spanning the entire range of n_f values (the change is only about 70% in the non-linear case). Too much emphasis cannot be placed on trends seen in this study. The differences seen here could also be due to the fact that ϵ_{f0} is further away from $(\epsilon_{fc})_{min}$ than δ is to $(\delta_c)_{min}$ (cf discussion of figures 8 and 10), in spite of the fact that we have chosen the initial slopes (for $\overline{V}$ close to 1) of the volume variation to be the same. We expect these differences to become more prominent with increasing non-linearity, but all the trends can be conclusively pinned down only after several other values of n, both positive and negative, have been studied.

The parameters in our model, i.e. ϵ_f, Δ and the slopes of the volume variations of these, characteristic of any particular system, can only be chosen by comparison with experiments. As a detailed application to a specific system, we now go back to the γ–α transition in cerium. In the following section we describe first the Martin and Allen (1985) work and then our own study of it. Although the calculations in both cases are crude compared to what we have described in the previous sections, they are useful, not only for highlighting the differences between the KVC model and ours but, more importantly, for pointing out the difficulties with fitting of experimental results in real systems.

5. The γ–α transition in cerium

5.1. The Kondo Volume Collapse model of Martin and Allen

The first-order, isostructural, γ–α transition in cerium (Lawson and Tang 1949), unique among elemental solids, has always attracted a lot of attention. Theoretical

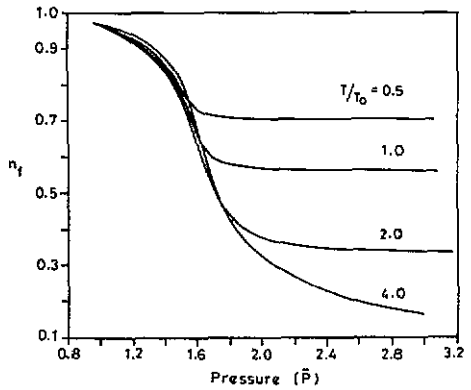

Figure 13. Valence versus pressure at four different temperatures when ϵ_f varies linearly with volume according to $\epsilon_f(\overline{V}) = \epsilon_f(0) + \delta D(1 - \overline{V})$; with $\delta = 1$ and $\epsilon_f(0) = -0.5D$; Δ is held fixed at $\Delta_0 = 0.08D$.

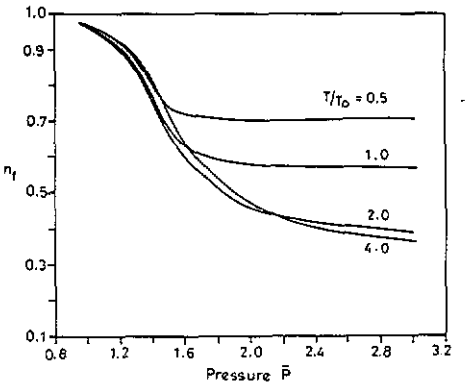

Figure 14. Valence versus pressure at different temperatures when ϵ_f varies non-linearly with volume, i.e. $\epsilon_f(V) = \epsilon_f(0)/\overline{V}^2$ with $\epsilon_f(0) = -0.5D$.

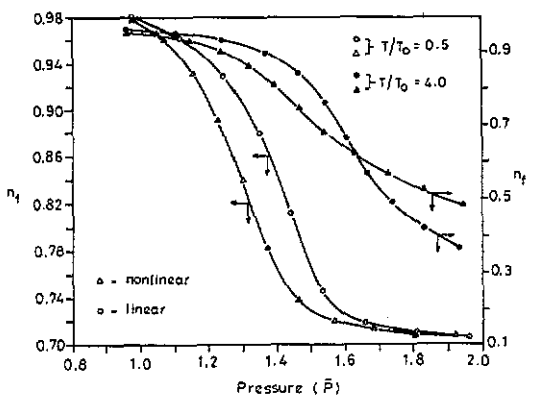

Figure 15. Detailed comparison of the linear (circles) and non-linear (triangles) volume variations of ϵ_f at low ($T < T_0$) as well as high temperatures. The initial response to pressure ($\overline{P}$ between 1 and 1.6) is more sensitive for the non-linear volume variation at all temperatures. In the linear case the overall change is smaller at low temperatures and larger at high temperatures.

efforts to understand this transition include the band-based models of Glotzel (1978) and Rainford and Edwards (1987) as well as the Kondo Volume Collapse model of Allen and Martin (1982), Martin and Allen (1983, 1985) and Lavagna *et al* (1982, 1983). Here we describe the work of Martin and Allen (1985) since this later work includes the effect of the orbital degeneracy of cerium.

Their model is based on two sets of experimental observations: (i) Contrary to the general correlation of reduced atomic volume with reduced f occupancy, several experimental techniques including L_{III} (Wohlleben and Rohler 1984) indicate that the γ and α phases are both integral-valent. Hence they can be described by the Kondo regime of the Anderson model or, equivalently, the Coqblin–Schrieffer (CS) model, which is the generalization to the case of large orbital degeneracy of the Kondo model. (ii) The Kondo coupling energy J varies rapidly with volume in

most cerium systems (Schilling 1979). Schilling has estimated that $J(V)$ is such that $d(\ln J)/d(\ln V)$ lies in the range -4 to -10, which presumably implies a highly non-linear volume dependence. The 15% volume change can thus cause large differences between the values of J in the two phases. To model this Allen and Martin (1982) use $J = 0.16/\overline{V}^6$, which for $\overline{V}$ close to 1, as in the case of the γ–α transition, can be approximated by $J = 0.16 + 0.96(1 - \overline{V})$. For the large-$N$ calculation (Martin and Allen 1985) they use $J = 0.15 + (1 - \overline{V})$.

The driving mechanism for the transition in the Kondo Volume Collapse model is the drastic volume dependence of the Kondo singlet stabilization energy $(-k_B\tilde{T}_0)$ arising from the strong volume dependence of J (taken to be dimensionless). $\tilde{T}_0$ is the Kondo temperature defined as

$$\tilde{T}_0 \equiv D\mathrm{e}^{-1/J}(\mathrm{e}J)^{1/N} \equiv T_0(\mathrm{e}J)^{1/N}. \tag{62}$$

The idea that Kondo energies drive the transition is also supported by two other facts: (i) the entropy change due to the multiplet–singlet transition, $k_B \ln(6)$, has a value $1.8k_B$, which is very close to the experimentally observed value of $1.54k_B$; (ii) the critical temperature T_c is of the order $\tilde{T}_0$. Also the estimates of $\tilde{T}_{0\alpha} = 4.7$ meV and $\tilde{T}_{0\gamma} = 66$ meV by Allen and Martin (1982) agree with those obtained from neutron scattering (Shapiro *et al* 1977) and correctly account for the change in the energy of $\simeq 60$ meV observed at the transition (Koskenmaki and Gschneidner 1978).

Martin and Allen write for their equation of state

$$P = B_N(1 - \overline{V}) - \frac{dE_G}{dJ}\frac{dJ}{dV} - \int_0^T dT' \frac{dC_v(V,T')}{dV}\left(1 - \frac{T}{T'}\right). \tag{63}$$

Here, as in (1), the first term is the elastic energy contribution, while the second and third terms come from the impurity free-energy contribution. Values of the normalized volume and bulk modulus V_N and B_N are chosen by them to be the average of the values for La and Pr (Scott 1978). For the ground-state energy E_G they use the result from systematic perturbation theory in $1/N$ (Rasul and Hewson 1983), the volume dependence of E_G coming in through J. For the actual calculations they use T_0 (the $N \to \infty$ limit for the Kondo temperature) rather than $\tilde{T}_0$ and set the ground-state energy to be

$$E_G = T_0 \equiv D\mathrm{e}^{-1/J}. \tag{64}$$

For the temperature-dependent part, i.e. the third term in (63), they retain the full finite-N form $\tilde{T}_0$ for the Kondo temperature, which comes in through the specific heat, and choose for the latter the result from the Bethe *ansatz* for the CS model (Rajan 1983). Starting from the equation of state (63) they study the γ–α phase transition by the standard equal-area construction (cf equations (4) and (5)) and obtain a phase boundary that is in qualitative agreement with experiment as shown in figure 16.

5.2. Further study of the γ–α transition and comparison with experiments

In our study of the details of the γ–α transition we continue to use the Anderson model, in order to be able to pinpoint the difference between the KVC description

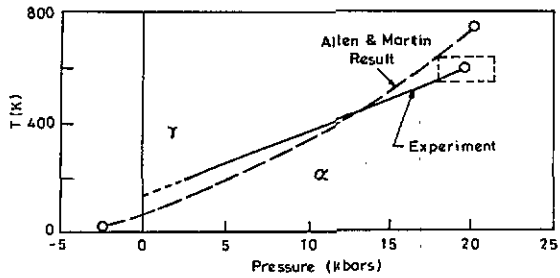

Figure 16. A portion of the phase diagram of Ce metal (King *et al* 1970) showing the γ–α phase boundary terminating in a critical point. The broken curve is the phase boundary calculated by Martin and Allen (1985) from their Kondo Volume Collapse model.

and ours. We incorporate the volume dependence through Δ, in accordance with the visualization of Martin and Allen, and also of Lavagna *et al*, that the γ–α transition is due to an increase in Δ, or equivalently of $J\,(\equiv -\Delta/|\epsilon_f|)$ with pressure. Experimental support of this idea comes from the neutron scattering results of Shapiro *et al* (1977), Rainford *et al* (1977) and Stassis *et al* (1979) and from the photoemission results of Croft *et al* (1981). The Kondo temperature of the high-pressure α phase is then very large since it depends exponentially on volume changes. Lavagna *et al* (1982, 1983) estimate T_0 to be 1000 K for Ce and 50 000 K for $CeAl_2$. Hence one should be able to treat this phase by a zero-temperature theory plus Fermi-liquid corrections to the free energy. On the other hand the γ phase has a small Kondo temperature (T_0 approximately 100 K) and may crudely be described by a high-temperature theory. At the simplest level, the phase boundary and critical point can be understood from the separate Helmholtz free energies of the two phases

$$F_\alpha(T,\overline{V}_\alpha) = \tfrac{1}{2}B_N V_N(\overline{V}_\alpha - 1)^2 + N_i[\Delta_\alpha \ln(\epsilon_f/D) - \tilde{T}_{0\alpha} - \tfrac{1}{2}\gamma_0 T^2] \tag{65}$$

$$F_\gamma(T,\overline{V}_\gamma) = \tfrac{1}{2}B_N V_N(\overline{V}_\gamma - 1)^2 + N_i[\Delta_\gamma \ln(\epsilon_f/D) - k_B T \ln 6]. \tag{66}$$

The $\Delta \ln(\epsilon_f/D)$ term is the extra contribution to the Kondo ground-state energy in the Anderson model, coming from virtual fluctuations into the singlet state (Krishnamurthy *et al* 1980); γ_0 is the coefficient of the specific heat at zero temperature, which has the Fermi-liquid value

$$\gamma_0 = \tfrac{1}{3}\pi^2 k_B^2 \frac{N-1}{N}\frac{1}{\Gamma(1+1/N)}\frac{1}{\tilde{T}_{0\alpha}} \tag{67}$$

and $\tilde{T}_{0\alpha}$ the Kondo temperature of the α phase is as defined in (62) but with a value of J appropriate to this phase. In our calculations too we have used the $N \to \infty$ form for the Kondo temperatures, i.e. $T_{0\alpha}$ and $T_{0\gamma}$, defined as in (64) but with the appropriate values of J in the two phases. The free-energy expressions (65) and (66) should provide reasonable descriptions of the α and γ phases for temperatures such that $T_{0\gamma} \ll T \ll T_{0\alpha}$. The first-order phase boundary is obtained from demanding that the pressure and Gibbs free energies of the two phases are equal (cf equations (4) and (5)). At any pressure P on this phase boundary, the volumes of the two phases are determined by the following conditions (from (5) and using (65) and (66)):

$$P = B_N(1-\overline{V}_\alpha) + \frac{N_i}{V_N}\left[\frac{\partial\Delta(\overline{V}_\alpha)}{\partial\overline{V}_\alpha}\ln\left(\frac{D}{\epsilon_f}\right) + \frac{\partial T_{0\alpha}}{\partial J}\frac{\partial J}{\partial\overline{V}_\alpha}\left(1 - \frac{\gamma_0 T^2}{2T_{0\alpha}}\right)\right] \tag{68}$$

$$P = B_N(1 - \overline{V}_\gamma) + \frac{N_i}{V_N}\left[\frac{\partial\Delta(\overline{V}_\gamma)}{\partial\overline{V}_\gamma}\ln\left(\frac{D}{\epsilon_f}\right)\right]. \tag{69}$$

As mentioned earlier, we have assumed that the volume dependence of J and hence of $T_{0\alpha}$ is due to a volume dependence of Δ. We take this to be of the form (slightly different from (23))

$$\Delta(\overline{V}) = \Delta_0 - \alpha(1 - \overline{V})\epsilon_f \tag{70}$$

which corresponds to a variation of J of the form

$$J(\overline{V}) = J_0 + \alpha(1 - \overline{V}) \tag{71}$$

in agreement with that of Martin and Allen (provided also that $J_0 = 0.15$ and $\alpha = 1$). Using (68) to (71) it is easy to see that $\overline{V}_\alpha(P,T)$ and $\overline{V}_\gamma(P)$ can be determined from

$$\overline{V}_\gamma = \left(1 - \frac{P}{B_N}\right) + \frac{N_i}{V_N B_N}\left[\alpha\epsilon_f \ln\left(\frac{D}{\epsilon_f}\right)\right] = \overline{V}_\alpha + \left[\frac{N_i}{V_N}\frac{\alpha}{B_N}\frac{T_{0\alpha}}{J_\alpha^2}\left(1 - \frac{\gamma_0(0)T^2}{T_{0\alpha}}\right)\right] \tag{72}$$

and these in turn are used in equations (4) and (5) to determine the phase boundary. Our results are shown as the full curve in figure 17. The broken curves are the Kondo temperatures of the two phases corresponding to the volumes determined from (72).

Needless to say, the approximations are consistent only in the middle of the phase diagram where $T_{0\alpha} \gg T \gg T_{0\gamma}$. They would be useless for understanding the critical points of the phase diagram, where the volumes and the Kondo temperatures of the γ and α phases become equal. This latter requirement implies that $T_{0\alpha}$ and $T_{0\gamma}$ should behave as shown schematically in figure 18. Comparing with figure 17 one can conclude that the approximation (66) for the γ-phase free energy in terms of the high-temperature limit may be acceptable but the approximation (65) for the α-phase free energy is obviously not very good. What is left out of (65) is the bootstrapping effect of increased temperatures, which bends the $T_{0\alpha}$ versus pressure curve from that in figure 17 to the one in figure 18. As the pressure and temperature increase along the phase diagram (figure 16), temperature-dependent terms in F_α must ensure that $\overline{V}_\alpha$ does not increase as much as expected on the basis of (72). Correspondingly $T_{0\alpha}$ would increase much less than in figure 17, making temperature effects more important, and so on.

In spite of the fact that this very important (for critical points) bootstrapping effect is missing in these crude calculations, we have found them to be useful in getting a zeroth-level qualitative understanding of many of the features of the KVC transition. Hence we have used them to study the following questions of interest with regard to choice of parameters for comparison with experiment.

(i) The importance (or lack thereof) of the $\Delta\ln(\epsilon_f/D)$ term in the free energy, since this term arises only in the Anderson model and is absent in the Kondo model.

(ii) The effect of a change in the elastic energy parameters, namely the bulk modulus and the reference volume, since this would change the balance between elastic and magnetic energy contributions.

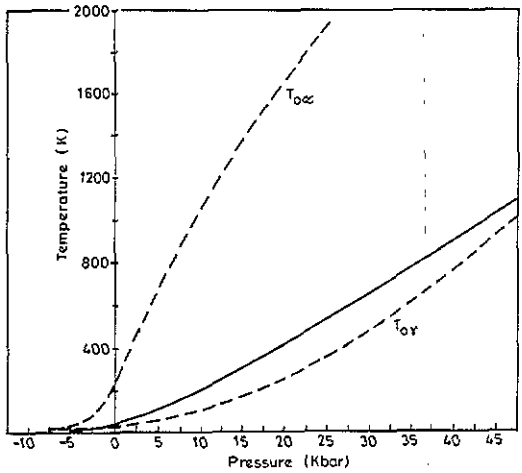

Figure 17. Phase boundary for the γ–α transition in Ce using approximate forms for the separate free energies of the two phases. Also shown in the figure are the corresponding Kondo temperatures of the two phases.

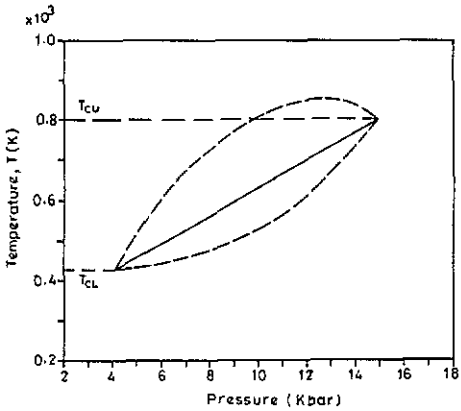

Figure 18. Schematic depiction of the modification to the behaviour of $T_{0\alpha}$ and $T_{0\gamma}$ (figure 17) required to understand the critical points in the phase diagram.

(iii) The difference between the results obtained using the leading order ($N \to \infty$) expression for T_0 and those obtained using the full expression $\tilde{T}_0$ because the Kondo temperature is a very sensitive function of volume. This question is of interest also for the understanding of the large-N expansion.

(iv) The role of particular forms of the volume dependence of the coupling constant and the consequence of changing either the slope α or the reference value J_0 in the form of $J(V)$ in (71).

As expected we find that while none of these are key features in obtaining a qualitative understanding of the valence-change transitions, comparisons with experimental phase diagrams become very difficult in view of the sensitive quantitative dependence of the results on these parameters. We discuss this in detail below.

Curve A in figure 19 is our equivalent of the Martin and Allen phase boundary

and serves as the reference curve. This has been obtained without including the $\Delta \ln(\epsilon_f/D)$ term in (65), specific to the Anderson model, along with their choice of parameters, i.e. $B_N = 280$ kbar, $V_N = 36$ Å^3, $J_0 = 0.15$, $\alpha = 1$ and T_0 rather than $\tilde{T}_0$ as the expression for the Kondo temperature. Curve B shows the effect of including the $\Delta \ln(\epsilon_f/D)$ term in the free energy. This term simply shifts the phase boundary towards negative pressures.

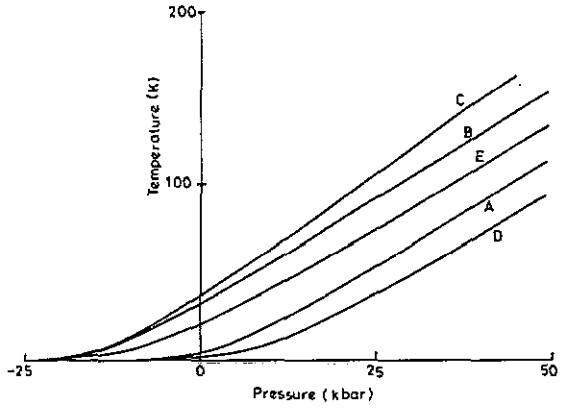

Figure 19. The γ–α phase boundary for different parameter values. The results illustrate the difficulty in making comparisons with experiment.

The values of B_N and V_N used by Martin and Allen are somewhat higher than those widely quoted in recent literature (Benedict *et al* 1986, Lavagna *et al* 1983). Curve C in figure 19 shows the effect of using $B_N = 239$ kbar and $V_N = 34.37$ Å^3 (Rose *et al* 1984). This changes the slope of the phase boundary and moves it towards lower pressures.

Since T_0 depends sensitively on volume, a small change in T_0 could make a large difference in the phase diagram. This is borne out by the difference in our results from using the finite-N form of the Kondo temperature $\tilde{T}_0$ (curve D). Crudely, a larger Kondo temperature, as in this case, seems to imply that a greater amount of pressure is needed to drive the transition at some fixed temperature. This result is to be expected in view of our picture of the transition as being one from the non-magnetic to the magnetic state of the impurity. Curve E is the result of the combined effects of the $\Delta \ln(\epsilon_f/D)$ term in the free energy and the choice of the finite-N form for the Kondo temperature, and illustrates the difficulty involved in fitting experimental results. Several combinations of the effects mentioned above can give equally good fits to a particular experimental phase boundary.

In order to study the effects on the phase diagram of changes in the volume dependence of $J(V)$, i.e. in the values of J_0 and α, it turns out to be important to get the phase boundary correctly, i.e. including critical points. For this purpose, as discussed earlier, one must use an impurity free energy that has a realistic temperature dependence (has the necessary bootstrapping effect): one that includes the Kondo-quenched, Fermi-liquid state at low temperatures and the destruction of the coherence of this state, leading to a free-moment behaviour at higher temperatures.

One way of doing the above is to use a full temperature-dependent free energy as described in sections 3 and 4. The other is to do as Martin and Allen have done, i.e. to write the free energy as the sum of the ground-state energy plus a temperature-dependent correction, which interpolates between low and high temperatures. For

the latter one can use the Bethe *ansatz* results for the CS model due to Rajan (1983), who has expressed his results for the specific heat in terms of an effective density of states $g(\epsilon)$ (to be obtained numerically)

$$C_v(T) = (N-1)k_B 2 \int_0^\infty d\epsilon \frac{(\epsilon/2k_BT)^2}{\cosh^2(\epsilon/2k_BT)} g(\epsilon) \tag{73}$$

$$F_i(T) = -k_BT(N-1) \int_{-\infty}^{\infty} d\epsilon\, g(\epsilon) \ln[1 + \exp(-\epsilon/k_BT)]. \tag{74}$$

Rather than using Rajan's numerical results for $g(\epsilon)$, we fitted the following analytical form for the scattering resonance:

$$g(\epsilon) = A \frac{T_0^4(a^4 + b^4)}{(\epsilon^2 - a^2T_0^2)^2 + b^4T_0^4}. \tag{75}$$

The parameters A, a and b can be determined from the conditions that the free energy at low and high temperatures have the correct behaviour, i.e.

$$F_i(T \to 0) = E_G = T_0 \tag{76}$$

$$F_i(T \to \infty) = -k_BT \ln(N) \tag{77}$$

and that the finite-temperature correction to the free energy at low temperatures leads to the Fermi-liquid expression for the specific heat coefficient (cf equation (67)). These conditions fix the coefficient A in (75) to be

$$A = \frac{1}{N\Gamma(1 + 1/N)} \frac{1}{T_0} \tag{78}$$

while a and b are solutions of the equations

$$a^2 = \frac{N\Gamma(1 + 1/N)}{N - 1} \frac{\sin(2z)}{\pi - z} \tag{79}$$

$$(\pi - z)\tan\left(\frac{z}{2}\right) = \pi^2 \left(\frac{\ln z}{\ln N}\right)^2 \frac{N-1}{N\Gamma(1+1/N)} \tag{80}$$

where $z = \tan^{-1}(b^2/a^2)$. The resulting density of states is compared with that of the Bethe *ansatz* for $N = 6$ in figure 20. Although the fit is not very good, it has the advantage of being easier to handle numerically.

Curve A in figure 21 shows the phase diagram obtained from the impurity free energy in (74) and using the above model density of states. It includes the $\Delta \ln(\epsilon_f/D)$ term, with the other parameters corresponding to the Allen and Martin choice. Thus it corresponds to curve B of figure 19. As in the earlier calculation, the $\Delta \ln(\epsilon_f/D)$ term is seen to shift the phase boundary to negative pressures. Furthermore, the fact that this phase boundary is terminated by critical points shows that our model density of states and corresponding free energy contain the bootstrapping effect responsible for producing the critical point.

Now consider the effect on this phase boundary of changes in the volume dependence of $J(V)$. A change in the reference value J_0 has a similar effect as that of

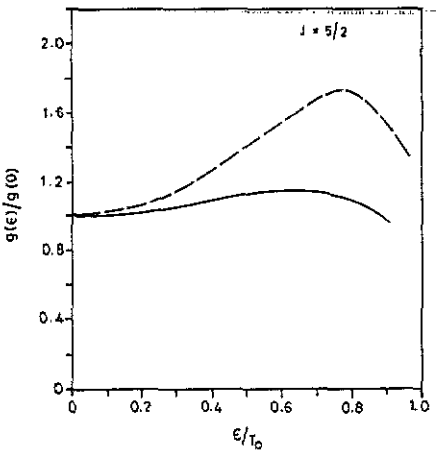

Figure 20. An approximate form for the density of states of the single-impurity scattering resonance (full curve) compared with the exact results from the Bethe *ansatz* (broken curve) for $N = 6$.

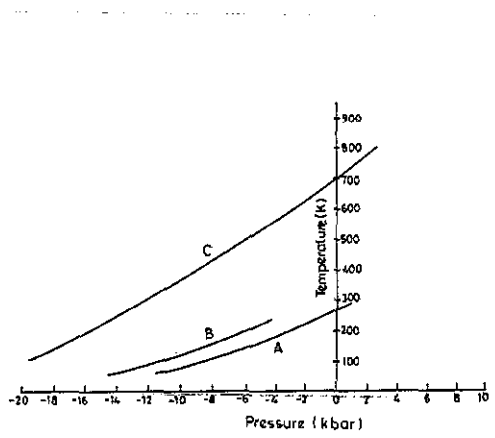

Figure 21. The γ–α phase boundary obtained by using the approximate form for the density of states in figure 20. The effect of variations in the parameter values describing the volume dependence of J is illustrated here (see text for details).

the $\Delta \ln(\epsilon_f/D)$ term, in that it shifts the phase boundary towards lower pressures (curve B in figure 21). On the other hand a change in the slope α expands the phase boundary, making discontinuous transitions possible over wider ranges of pressure and temperature. The change in α also shifts the phase boundary towards higher temperatures. This trend has already been demonstrated in sections 3 and 4 (figure 9) as well as in the simpler calculation presented earlier in this section (figure 19). The effect of changes in α is brought out in more detail in figure 22. Here we plot the upper and lower critical temperatures as a function of α. Actually these are the two branches of one smooth curve $\alpha_c(T)$, which was obtained in the full calculations described in section 4. The fact that the same qualitative trends are seen in the simpler calculations described in this section as in sections 3 and 4 implies that two important conclusions can be drawn. The competing effects of different contributions to the free energy resulting in ambiguities with regard to fitting experimental results seen here is also true of the results in section 3 and 4. More importantly, it demonstrates that the only crucial features necessary to describe the first-order phase boundary and critical point are the non-linear volume dependence of the free energy and the bootstrapping effect of high temperatures.

Our results make clear that, at the quantitative level, the phase diagram of the KVC model is affected substantially by the variety of factors that we have considered. As discussed in detail in the following section, this is probably the reason why several other explanations in the literature, for phase diagrams, different from the one discussed here and of varying levels of sophistication, have met with just as much success. In particular, this is probably the reason for the discrepancy between the theory of Lavagna *et al* (1983) for $CeAl_2$ and experimental results. They predict a first-order transition at all temperatures but in reality the transition is almost always continuous (Vedel *et al* 1986, Penney *et al* 1981). Clearly the choice of parameters necessary to fit a theoretical phase diagram to experimental data is not unambiguous and can be done believably only when some of these parameters can be fixed else-

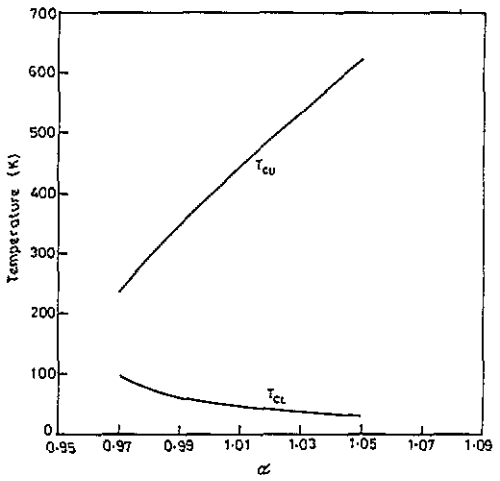

Figure 22. Plot of the upper and lower critical temperatures T_{cu} and T_{cl} as a function of α, the slope of the volume variation of J. These are two branches of the full curve $\alpha_c(T)$ shown in figure 9.

where, namely by good theoretical calculations for the results of other experiments in the same systems.

6. Discussion and summary

Our calculations have left out several effects clearly present in mixed-valent systems. Two of the important ones are Coulomb corrections and effects due to strong coupling to the lattice. The large volume difference between the two valence configurations and the highly localized nature of the 4f states of the impurity lead to strong screening and on-site correlation effects and also to strong coupling to the lattice. Part of these effects, those which can be taken into account by a renormalization of the Anderson model parameters, is included, since in our calculation these parameters are phenomenological (Razafimandimby *et al* 1984). It is actually rather difficult to separate the contributions of these two effects. Neither can be expected to make any qualitative difference but they would further complicate quantitative fits to experiments. Mannheimer and Parks (1979), based on their study of cerium systems, have conjectured that the bootstrapping effect responsible for the valence transition in these systems is lattice-mediated rather than through Coulomb forces.

Coulomb forces are known to play an important role in metal–insulator transitions. In many alloy systems, e.g. SmS_xSe_{1-x}, valence transitions, continuous as well as discontinuous, are accompanied by a change from metallic to non-metallic behaviour (Wohlleben 1976). They are important because the 4f levels are highly localized, having large correlation energies, and hence significant screening effects can be present when the valence changes. One way to account for this effect is to include a 'Falicov–Kimball' term in the Hamiltonian (Falicov and Kimball 1969). In a mean-field approximation, this means we should include a term $\lambda n_f(1 - n_f)$ in the free energy (for $\lambda < 0$ this term is attractive and favours valence changes) and do a self-consistent calculation for the f-level position. Bowen and Lady (1984) have made a Green function treatment of this Hamiltonian and conclude that Coulomb correlations by themselves are not key ingredients to understanding valence-change transitions.

The effect of coupling to the lattice in the form of local polarons has been studied in detail by Hewson and Newns (1979, 1980), who conclude that the dominant effect of this coupling, in the range of frequencies relevant to mixed-valent systems, would be to renormalize and reduce inter-site hopping rather than to reduce Δ as claimed earlier by Sherrrington and Von Molnar (1975). Their result can thus be used as another argument supporting the treatment of mixed-valent systems as collections of non-interacting impurities. From their work one expects that local polaron effects, if any, are negligible.

In summary, we have presented a semi-phenomenological model for phase transitions in mixed-valent systems that is a generalization of the Kondo Volume Collapse model of Allen and Martin. It is based on competition effects between magnetic and elastic energy contributions to the free energy and is capable of providing a unified description of very diverse responses to pressure seen experimentally in these systems. We have studied the role of different contributions to the free energy and their dependences on parameter values. We have found that the only crucial feature necessary to describe valence-change transitions is that the free energy depends non-linearly on volume. The precise source of the non-linearity seems to be irrelevant so that comparisons with experiment are necessarily ambiguous.

This fact explains the apparent success of several other approaches to the equation of state in mixed-valent systems, which keep only one or the other source of non-linearity. Varma and Heine (1975) in their calculation of the equation of state of samarium chalcogenides explicitly keep non-linear effects through coupling to phonons, but neglect completely effects due to the hybridization width. They obtain fits to within 20% of experimental results. Non-linear effects coming from the lattice have also been included by Jayaraman *et al* (1974) using an empirical relation connecting bulk moduli at different volumes. We have made preliminary calculations in which we replace the linear term in the pressure–volume relationship with the non-linear scaling form of Rose *et al* (1984). We have found that, when both elastic and magnetic contributions are non-linear and are present together, then for the same set of parameters and external conditions like temperature, pressure, etc, the valence transition shows a tendency to become less discontinuous. This result needs to be explored further. Our treatment is restricted to only those systems in which one of the two configurations involved in valence fluctuations is magnetic, and therefore does not cover Tm based systems.

References

Allen J W and Martin R H 1982 *Phys. Rev. Lett.* **49** 1106

Anderson P W 1961 *Phys. Rev.* **124** 41

—— 1981 *Valence Fluctuations in Solids* ed L M Falikov, W Hanke and M B Maple (Amsterdam: North-Holland) p 451

Batlogg B, Jayaraman A, Murgai V, Gupta L C, Parks R D and Croft M 1982 *Valence Instabilities* ed P Wachter and H Boppart (Amsterdam: North-Holland) p 229

Benedict U, Grosshans W A and Holzapfel W B 1986 *Physica* B **144** 14

Bowen S P and Lady S C 1984 *J. Appl. Phys.* **55** 1925

Chandran L 1987 *PhD Thesis* Indian Institute of Science, Bangalore

Chandran L and Krishna-murthy H R 1987 unpublished

Chatterjee A, Singh A K and Jayaraman A 1972 *Phys. Rev.* B **6** 2285

Coleman P 1984 *Phys. Rev.* B **29** 3035

Croft M, Hodges J A, Kemly E, Krishnan A, Murgai V and Gupta L C 1982a *Phys. Rev. Lett.* **48** 826

Croft M, Segre C V, Hodges J A, Krishnan A, Murgai V, Gupta L C and Parks R D 1982b *Valence Instabilities* ed P Wachter and H Boppart (Amsterdam: North-Holland) p 121
Croft M, Weaver J H, Peterman D J and Franciosi A 1981 *Phys. Rev. Lett.* **46** 1104
Evdokimova V V and Genshaft Y S 1965 *Sov. Phys.–Solid State* **6** 1941
Falicov L M and Kimball J 1969 *Phys. Rev. Lett.* **22** 997
Glotzel D 1978 *J. Phys. F: Met. Phys.* **8** L163
Gupta L C, Murgai V, Yeshrun Y and Parks R D 1982 *Valence Instabilities* ed P Wachter and H Boppart (Amsterdam: North-Holland) p 225
Hewson A C and Newns D M 1979 *J. Phys. C: Solid State Phys.* **12** 1665
—— 1980 *J. Phys. C: Solid State Phys.* **13** 4477
Hewson A C, Newns D M, Rasul J W and Read N 1985 *J. Magn. Magn. Mater.* **47/48** 374
Holland-Moritz E 1985 *J. Magn. Magn. Mater.* **47/48** 131
Jayaraman A 1972 *Phys. Rev. Lett.* **29** 1674
—— 1979 *Handbook of Physics and Chemistry of Rare-Earths* ed K A Gschneidner and L Eyring (Amsterdam: North-Holland) p 575
Jayaraman A, Singh A K, Chatterjee A and Usha Devi S 1974 *Phys. Rev.* B **9** 2513
King E, Lee J A, Harris I R and Smith T F 1970 *Phys. Rev.* B **1** 1380
King Jr H E, Laplaca S J, Penney T and Fisk Z 1981 *Valence Fluctuations in Solids* ed L M Falikov, W Hanke and M B Maple (Amsterdam: North-Holland) p 333
Koskenmaki D C and Gschneidner K A 1978 *Handbook of Physics and Chemistry of Rare-Earths* ed K A Gschneidner and L Eyring (Amsterdam: North-Holland) p 337
Krishna-murthy H R, Wilkins J W and Wilson K G 1980 *Phys. Rev.* B **21** 1044
Lavagna M, Lacroix C and Cyrot M 1982 *Phys. Lett.* **90A** 210
—— 1983 *J. Phys. F: Met. Phys.* **13** 1007
Lawrence J M, Croft M C and Parks R D 1975 *Phys. Rev. Lett.* **35** 289
Lawson A W and Tang T Y 1949 *Phys. Rev.* **76** 301
Leger J M, Oki K, Ravot D, Rossat-Mignod J and Vogt O 1985 *J. Magn. Magn. Mater.* **47/48** 277
Mannheimer M A and Parks R D 1979 *Phys. Rev. Lett.* **42** 321
Martin R M and Allen J W 1983 *J. Magn. Magn. Mater.* **31–34** 473
—— 1985 *J. Magn. Magn. Mater.* **47/48** 257
Mattens W C M, Holscher H, Tuin G J M, Moleman A C and de Boer F R 1980 *J. Magn. Magn. Mater.* **15–18** 982
McWhan D B and Remeika J P 1970 *Phys. Rev.* B **2** 3734
Mignot J M and Wittig J 1982 *Valence Instabilities* ed P Wachter and H Boppart (Amsterdam: North-Holland) p 203
Neumann G, Pott R, Rohler J, Schlabitz W, Wohlleben D and Zahel H 1982 *Valence Instabilities* ed P Wachter and H Boppart (Amsterdam: North-Holland) p 87
Nowik I 1986 *Phys. Rev.* B **33** 617
—— 1987 *J. Magn. Magn. Mater.* **63/64** 615
Penney T, Barbara B, Melcher R L, Plaskett T S, King Jr H E and La Placa S J 1981 *Valence Instabilities* ed P Wachter and H Boppart (Amsterdam: North-Holland) p 341
Perscheid B, Sampathkumaran E V and Kaindl G 1985 *J. Magn. Magn. Mater.* **47/48** 410
Rainford B D, Buras B and Lebech B 1977 *Phys. Lett.* **86–88B** 41
Rainford B D and Edwards D M 1987 *J. Magn. Magn. Mater.* **63/64** 557
Rajan V T 1983 *Phys. Rev. Lett.* **51** 308
Ramakrishnan T V 1981 *Valence Fluctuations in Solids* ed L M Falikov, W Hanke and M B Maple (Amsterdam: North-Holland) p 13
Rasul J W and Hewson A C 1983 *J. Phys. C: Solid State Phys.* **16** L933
Razafimandimby H, Fulde P and Keller J 1984 *Z. Phys.* B **54** 111
Read N and Newns D M 1983a *J. Phys. C: Solid State Phys.* **16** 3273
—— 1983b *J. Phys. C: Solid State Phys.* **16** L1055
Rohler J, Krill G, Kappler J P, Ravet M F and Wohlleben D 1982 *Valence Instabilities* ed P Wachter and H Boppart (Amsterdam: North-Holland) p 215
Rose J H, Smith J R, Guinea F and Ferrante J 1984 *Phys. Rev.* B **29** 2963
Sampathkumaran E V 1981 *J. Phys. C: Solid State Phys.* **14** L237
Sampathkumaran E V, Vijayaraghavan R, Gopalakrishnan K V, Pilley R G and Devare H G 1981 *Valence Fluctuations in Solids* ed L M Falikov, W Hanke and M B Maple (Amsterdam: North-Holland) p 193
Schilling J S 1979 *Adv. Phys.* **28** 657

Schmiester G, Perscheid B, Kaindl G and Zukrovsky J 1982 *Valence Instabilities* ed P Wachter and H Boppart (Amsterdam: North-Holland) p 219
Scott T E 1978 *Handbook of Physics and Chemistry of Rare-Earths* ed K A Gschneidner and L Eyring (Amsterdam: North-Holland) p 701
Segre C U, Croft M, Hodges J A, Murgai V, Gupta L C and Parks R D 1982 *Phys. Rev. Lett.* **49** 1947
Shapiro S M, Axe J D, Birgeneau R J, Lawrence J M and Parks R D 1977 *Phys. Rev.* B **16** 2225
Sherrington D and Von Molnar S 1975 *Solid State Commun.* **16** 1347
Spain I L, Steglich F, Rauchschwalbe U and Hochheimer H D 1986 *Physica* B **139/140** 449
Stassis C, Gould T, McMasters O D, Gschneidner Jr K A and Nicklow R M 1979 *Phys. Rev.* B **19** 5746
Thompson J D, Fisk Z, Lawrence J M, Smith J L and Martin R M 1983 *Phys. Rev. Lett.* **50** 1081
Varma C M and Heine V 1975 *Phys. Rev.* B **11** 4763
Vedel I, Redon A M, Leger J M, Mignot J M and Flouquet J 1986 *J. Magn. Magn. Mater.* **54–7** 361
Wohlleben D 1976 *J. Physique Coll.* **37** C4 231
Wohlleben D and Rohler J 1984 *J. Appl. Phys.* **55** 1904
Wortmann G, Syassen K, Frank K H, Feldhaus J and Kaindl G 1982 *Valence Instabilities* ed P Wachter and H Boppart (Amsterdam: North-Holland) p 159